Excited-state dynamics and energy transfer of +4 curium in cerium tetrafluoride

G. K. Liu and James V. Beitz
Argonne National Laboratory, Argonne, Illinois 60439
(Received 27 November 1989)

Energy-transfer dynamics of $5f$ states of +4 curium in cerium tetrafluoride have been investigated for the first time. Emission from the lowest energy component of the second $J=1$ multiplet was studied using time- and frequency-resolved laser-induced fluorescence. The observed dynamics were complex due, in part, to the strong ion-lattice coupling and the dense f-state energy-level structure of Cm^{4+}. The influence of experimental parameters such as excitation frequency, excitation intensity, sample temperature, and prior optical irradiation on the observed nonexponential fluorescence decays was determined. The observed $5f$-state dynamics of 0.1 at. % Cm^{4+}:CeF_4 are well fit by a cross-relaxation model, except at low temperature and high excitation intensity, where photoinduced site distortion and ground-state depletion via a two-photon process occurred. In this case, the initial fluorescence decay rate of Cm^{4+} on one of the two metal-ion sites was reduced in comparison with the rate observed at lower excitation intensity. A cross-relaxation model incorporating exciton-exciton annihilation was necessary to describe the fluorescence dynamics of 5 at. % Cm^{4+}:CeF_4. The derived energy-transfer rates for $5f$ states of Cm^{4+} via cross relaxation and up conversion are two orders of magnitude higher, at equal ion densities, than those of lanthanide-ion $4f$ states and approach those of transition-metal-ion d states.

I. INTRODUCTION

Studies of dynamical processes, such as transfer of excitation energy among optically active ions in solids, are of fundamental importance in understanding the nature of physical interactions and provide direct measurements of ion properties. Unlike the rare-earth ($4f$) ions, whose dynamical processes have been investigated extensively,[1-4] the actinide ($5f$) ions are unexplored because they are not commonly available and their electronic-energy-level structures are still not fully understood.[5-8] Investigations of actinide-ion $5f$ states are of considerable interest as the dynamical properties of $5f$ states are likely to be intermediate between those of lanthanide $4f$ and transition-metal d states.

Among all energy-transfer processes, those involving additional electronic levels, such as cross relaxation and up conversion, are of particular significance because they can strongly influence the fluorescence yield and quantum efficiency of optical systems. The time- and frequency-resolved fluorescence-decay technique provides a powerful probe for these energy-transfer processes and others that cause observable changes in dynamical characteristics, such as nonexponentiality and spectral migration.[9-13]

Cross relaxation is a self-trapping process in which donors act as their own acceptors.[9-11] In cross relaxation, an excited ion interacts with and gives up a part of its excitation energy to a neighboring ion in a lower state. The net result is that both ions end up in one or two different intermediate energy states, thereby quenching the fluorescence from the originally excited state. In resonant cross relaxation, the sum of the energies of the intermediate states is equal to the initial excitation energy. In the nonresonant case, energy conservation is achieved via creation or destruction of phonons. Cross relaxation has been observed in a variety of rare-earth materials.[14-17] The well-known Inokuti-Hirayama model[18] is often used to interpret the experimental observation of nonexponential fluorescence decays due to the cross relaxation.

Up conversion via so-called exciton-exciton annihilation is a special type of cross-relaxation process in which two identical ions, both initially in the excited state, interact. The result is promotion of one ion to a higher excited state via loss of energy from the other ion. Any energy mismatch is accommodated via creation or destruction of phonons.[3,11,13] Exciton-exciton annihilation is well known in organic molecular solids, where both triplet and singlet annihilation occurs.[19-22] In transition-metal systems, exciton-exciton annihilation has been observed in Mn^{2+} compounds.[23,24] For highly localized $4f$ states, annihilation of Frenkel excitons has been observed in $NdCl_3$,[25] $TbPO_4$,[26] and TbF_3 (Ref. 27) compounds. These studies of $4f$ states required relatively high-excited-state densities due to the weak coupling between the rare-earth ions that results in low exciton mobility. Analogous processes have been studied in dilute rare-earth compounds.[28-31] The first observation of exciton-exciton annihilation effect in rare-earth compounds was reported for Er^{3+} doped in fluorite crystal such as Er^{3+}:BaF_2.[28] Although no energy-transfer rates were given, exciton-exciton annihilation effect has been reported for 1 at. % Pr^{3+}:LaF_3 and Pr^{3+}(Nd^{3+}):$LaCl_3$ compounds.[29,30] In these cases, the exciton-exciton annihilation was interpreted as an up-conversion process between two neigh-

boring active ions both in the excited state. Whichever terminology is appropriate, the observed nonexponential decays, which depend nonlinearly on the excitation intensity, can be analyzed with simple decay rate equations.

For actinide doped solids, most reported work has centered on the determination of the electronic-energy-level structure.[5–8] Little is known about the dynamical properties of the excited $5f$ states of the actinides in solids. Large electron-phonon interaction has been previously reported in Np^{3+}:$LaCl_3$, based on temperature-dependent fluorescence line narrowing measurements.[32] A recent study has provided evidence of energy transfer between U^{4+} ions in different sites in a U^{4+}:$ThBr_4$ compound.[33] With tetravalent actinide ions doped in CeF_4, we are carrying out systematic spectroscopic studies of electronic-state energy-level structure as well as determining the dynamical properties of excited $5f$ states. Our recent results[34] have shown that the spectra and dynamics of the $+4$ actinide ions can be quite complicated due to ion-ion and ion-lattice interactions arising from the comparatively dense $5f$-state structure of transamericium $+4$ ions. Excitation-intensity-, excitation-frequency-, and temperature-dependent nonexponential fluorescence decays have been observed at actinide-ion concentrations as low as 0.1 at. %. In the case of Cm^{4+}:CeF_4, efficient two-photon excitation and laser-induced site distortion due to strong ion-lattice coupling have been observed. These phenomena have important roles in the dynamics of the observed fluorescence decays.

Because of greater radial extent of $5f$ electron wave functions, with respect to those of the shielding $6s$ and $6p$ shells, the coupling between $5f$ states of actinide ions and the surrounding lattice is expected to be significantly stronger than is the case for $4f$ states of $+3$ lanthanide ions.[5,7,8] The mobility of excited-state energy among $5f$ electron states is expected, therefore, to be intermediate between that found for $4f$ states of rare-earth ions and d states of transition-metal ions. Furthermore, because of increased spin-orbit interaction and reduced electronic repulsion of the $5f$ electrons,[5,8] J splittings of actinide $5f$ states are large as the overall $5f$ electronic-energy range is reduced in comparison with that of $4f$ electrons, for the same number of f electrons. This results in a high density of energy states and an increased probability of overlap between a vibronic band and the next higher-lying purely electronic state. Overall, energy-transfer processes such as cross relaxation and up conversion are more likely to dominate the observed dynamics of actinide compounds than is the case in rare-earth materials.

In this paper, we report the first detailed study of the dynamics of excited $5f$ states of a transplutonium $+4$ ion. A brief description of the energy-level structure of Cm^{4+} in CeF_4 is presented in Sec. III and experimental results are summarized in Sec. IV. The observed nonexponential fluorescence decays in 0.1 at. % Cm^{4+}:CeF_4 are analyzed in Sec. V, based on a model involving cross relaxation influenced by laser-induced site distortion at high excitation densities. In Sec. VI, the extremely nonexponential decays in 5 at. % Cm^{4+}:CeF_4 are interpreted by a model incorporating exciton-exciton annihilation, cross relaxation, and trapping to defects.

II. EXPERIMENTAL APPARATUS AND SAMPLE PREPARATION

A tunable dye laser (Molectron DL-16P), pumped by a Q-switched, frequency-tripled, Nd:YAG laser (Quanta-Ray DCR-2A) was used as the excitation source. For higher-resolution work, the pressure of nitrogen gas in the oscillator chamber containing the grating, an etalon, and a prism-beam expander was varied, under the control of a computer-generated voltage ramp, using an analog pressure controller (MKS 250B) with a capacitance manometer (MKS 220BA) pressure transducer.[35] The sample temperature was varied using a continuous flow, heat-exchange gas cryostat equipped with fused-silica windows providing high transmission from 200 to 3500 nm (Oxford CF204 with DTC2 temperature controller). The fluorescence from the sample was directed onto long-band pass optical filters (Schott KV series), dispersed using a 1-m focal-length monochromator (Engis 1000), and detected using cooled GaAs (RCA 31034) or S-1 (Hamamatsu 7102) photomultipliers. The input resistance of a buffer amplifier connected to the photomultiplier was varied to provide a range of detection-system response times.

Fluorescence dynamics were measured using a transient recorder (LeCroy TR8818) connected to a minicomputer that carried out add-to-memory signal averaging of the transient recorder data. Such signal averaging was carried out over a few to as many as 2048 laser pulses. The data were transferred to a local area VAX cluster where a nonlinear least-squares fitting procedure was used to analyze the observed fluorescence decays. The decay models used are described later.

Excitation and emission spectra were recorded using as many as three boxcars as gated integrators with different gate delays. A pyroelectric detector (Molectron J3-05) and a boxcar integrator were used to acquire the dye laser-pulse energy and the fluorescence spectra were normalized to it. The outputs of the boxcars were digitized using a 12 bit backplane ADC (Data Translation DT2782) in the minicomputer. The optogalvanic effect in a uranium hollow cathode discharge, the uranium line atlas of Palmer *et al.*,[36] and the fringe pattern from a solid etalon were used for wavelength calibration of excitation spectra. Efforts to detect longer wavelength fluorescence were made using CaF_2 lenses, GaAs, Si, and Ge disks as long pass filters, and a 1-μs response time, 3-mm diameter, InSb detector that was cooled to 77 K.

The Cm^{4+} in CeF_4 samples were prepared using ^{248}Cm obtained from the Transplutonium Production Program of the U.S. Department of Energy. The method used started with co-precipitation of Cm^{3+} and Ce^{3+} from aqueous solution using added hydrofluoric acid. The stated Cm and Ce values for each sample are the concentrations of Cm and Ce in the aqueous solution prior to precipitation. The solid precipitate was dried at 110 °C in air and transferred to a sapphire crucible that was heated in a nickel tube containing anhydrous HF gas to remove residual water. The tube was then evacuated, filled with excess high-purity fluorine gas, and heated. The fluorine

had been fractionally distilled at cryogenic temperatures to remove impurities such as oxygen.[37] The nickel tube was opened in a dry nitrogen-filled controlled atmosphere glovebox and a portion of the resulting white, free-flowing powder was transferred to a sample cell. The sample cell was then evacuated, back filled with a few kPa of He gas, and flame sealed. The sample cells were made from General Electric type 214 water-free quartz. This type of quartz was used to ensure freedom from hydroxyl overtone absorption in the near infrared and good transparency out to 3700 nm. The sample cells tapered down to a circa 1-mm-inner-diameter capillary end that contained the powdered sample. A portion of the $Cm_{0.001}Ce_{0.999}Fe_4$ (i.e., 0.1 at. % Cm^{4+}:CeF_4) sample underwent analysis by x-ray powder diffraction to verify that the structure of the material was the same as a sample of undoped CeF_4.

III. SPECTRAL CHARACTERISTICS

A. Site symmetry

The host material CeF_4 is isostructural with a series of AnF_4 compounds such as UF_4 (Ref. 38) and BkF_4 (Ref. 39). In these compounds, the metal ion sits on either of two sites, one of C_2 symmetry and the other of C_s symmetry. Each metal ion is surrounded by eight fluorine ions arranged in a slightly distorted antiprism configuration. When Cm^{4+} ions substitute for Ce^{4+} ions in CeF_4, the actinide ions can occupy two sites of different symmetry and nonequivalent local environments. Consequently, differences in energy-level structure and dynamics are expected for Cm^{4+} ions on the two crystallographic sites in Cm^{4+}:CeF_4 samples.

B. Selective excitation

High-resolution laser excitation was utilized to unravel the resulting complex multisite spectra of Cm^{4+}:CeF_4 and to investigate the dynamics of the excited f-states of the actinide ion on the nonequivalent sites. The two sites are termed arbitrarily site A and site B because it is not possible to spectroscopically determine the site symmetry C_s or C_2 from fluorescence measurements on the powdered samples. Because of increased spin-orbital coupling and configuration interaction,[5,7,8] the standard Russell-Saunders SLJ terminology, applicable to many lanthanide $4f$ states, is inappropriate for actinide $5f$ states except that J is still a good quantum number. In the following, $5f$ states of Cm^{4+} are labeled by their J value. The observed electronic states and vibronic bands are shown in Fig. 1. The positions of the lower-lying energy levels and the dynamical studies were carried out using fluorescence from the second $J=1$ state, which is the only $5f$ state of Cm^{4+} from which emission was observed.

The observed excitation and emission spectra of the nonequivalent Cm^{4+} ion sites in Cm^{4+}:CeF_4 consisted of both electronic and vibronic transitions. As shown in Fig. 2, the excitation spectra of sites A and B in the 0.1 at. % Cm^{4+} sample at 4 K, for the transition from the

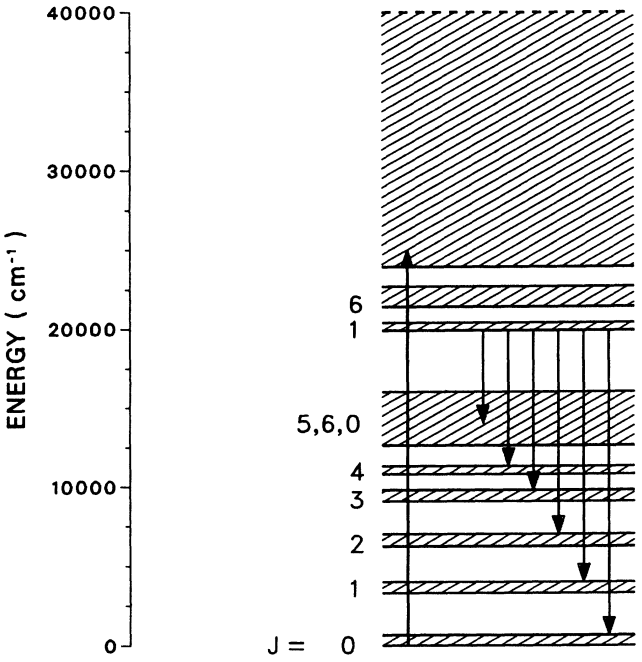

FIG. 1. Energy-level diagram for Cm^{4+}:CeF_4. Energy levels up to 26000 cm^{-1} were determined from laser excitation experiments. The energy extent of each observed multiplet, including vibronic bands, is shaded with diagonal lines and its predicted (Ref. 51) J value is shown at the left. All observed fluorescence, shown as downward pointing arrows, comes from the second $J=1$ state. A high density of states is predicted (Ref. 51) above 26000 cm^{-1}.

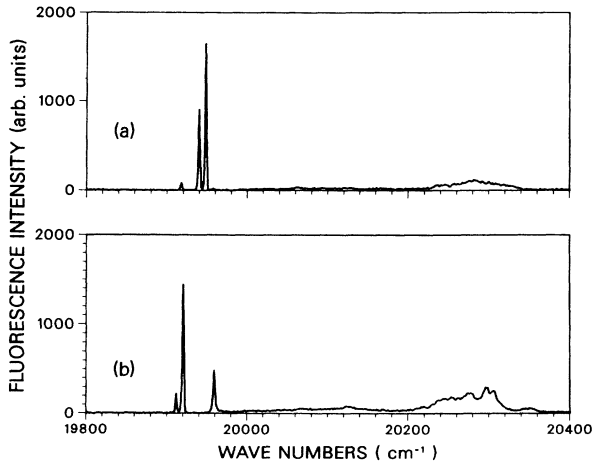

FIG. 2. Site-resolved fluorescence excitation spectra of the second $J=1$ multiplet of 0.1 at. % Cm^{4+} CeF_4. Emission from a single site was monitored. Subplot (a) is for Cm^{4+} on site A and subplot (b) is for Cm^{4+} on site B. The lowest purely electronic component (19916 cm^{-1} for site A and 19911 cm^{-1} for site B) in this multiplet is the emitting level whose dynamics have been investigated in this work. The broad band extending to higher energy is attributed to vibronic transitions.

$J=0$ ground state to the second $J=1$ excited multiplet, contain three purely electronic lines at lower energy and broad bands at higher energy that are attributed to vibronic transitions. The lowest energy line in each site-resolved spectrum is the only observed metastable emitting level of Cm^{4+} in this compound and the excited-state dynamical studies were carried out using this state.

C. Vibronic transitions

Because of the radial extent of the $5f$ orbitals, ion-lattice interaction resulting in intense and broad vibronic transitions are expected in actinide compounds. In Cm^{4+}:CeF_4, vibronic transitions with peak intensities comparable to the narrow zero-phonon lines were indeed observed (see Figs. 2 and 3). The vibronic bands are sufficiently intense to obscure some purely electronic lines. Figure 3 shows the emission spectra of 0.1 at.% Cm^{4+}:CeF_4 (sites A and B) from the metastable emitting state to the lowest-energy $J=1$ multiplet. The two narrow lines at higher emission energy are purely electronic transitions, and the broad bands at lower emission energy are vibronic structures associated with the lowest energy $J=1$ multiplet.

D. Laser-induced site distortion

In addition to vibronic transitions, ion-lattice interactions can also cause structural distortion, i.e., a conversion of the electronic energy of the excited ion into the elastic energy of the crystal configuration. In the dilute compound 0.1 at.% Cm^{4+}:CeF_4 distortion of site A Cm^{4+} has been observed after site-selective laser excitation and details will be given in a separate paper.[40] The laser-induced site distortion is stable below 70 K. On the distorted site, Cm^{4+} ions have different excitation and emission frequencies resulting from the perturbed crystal field accompanying the site distortion. The observed excitation-energy shift for the metastable emitting level was 3 cm^{-1}, whereas the three purely electronic components of this multiplet were shifted by an average of 12 cm^{-1}.

Understood as an excited-state Jahn-Teller effect,[41,42] the site distortion could occur in the emitting multiplet or in the low-energy J multiplets after a radiative transition. In the first case, the site distortion quenches fluorescence. In either case, the site distortion could impact energy transfer because the distortion causes changes in the energy-level structure of the ions on the distorted site.

E. One- and two-photon excitation

Efficient two-photon excitation has been observed in Cm^{4+}:CeF_4 as evidenced by a supralinear dependence of a fluorescence intensity on the intensity of pumping laser (see Fig. 4) and emission from Cm^{4+} on site A (19 916 cm^{-1}) and site B (19 911 cm^{-1}) following excitation in the 14 830–14 880-cm^{-1} region.[43] Using a pump laser near 20 000 cm^{-1} to excite the metastable $J=1$ emitting state, absorption of two photons by a single Cm^{4+} ion will put 40 000 cm^{-1} of energy into the ion. Emission was observed only from the metastable $J=1$ state, which provides evidence of very rapid nonradiative relaxation from the Cm^{4+} states above 20 000 cm^{-1}. The probability of direct two-photon absorption (even with resonant enhancement due to the real states near 20 000 cm^{-1}) is negligible in comparison with the probability of sequential absorption of two photons by a single Cm^{4+} ion.[44,45]

The observable effect of the two-photon excitation process in Cm^{4+}:CeF_4 is the population of the metastable emitting level of Cm^{4+}. Using excitation near 20 000

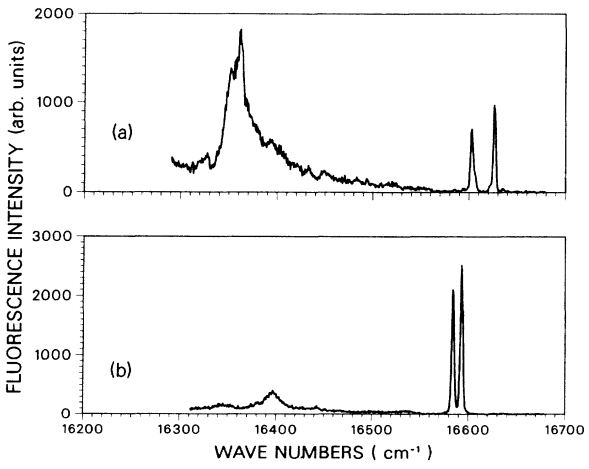

FIG. 3. Site-resolved fluorescence emission spectra for the transition from the emitting $J=1$ level (see Fig. 2) to the lower-lying $J=1$ multiplet of 0.1 at.% Cm^{4+}: CeF_4 at 4 K. Subplot (a) is for site A Cm^{4+} and subplot (b) is for site B Cm^{4+}. The broad, structured, band extending to lower energy is attributed to vibronic transitions.

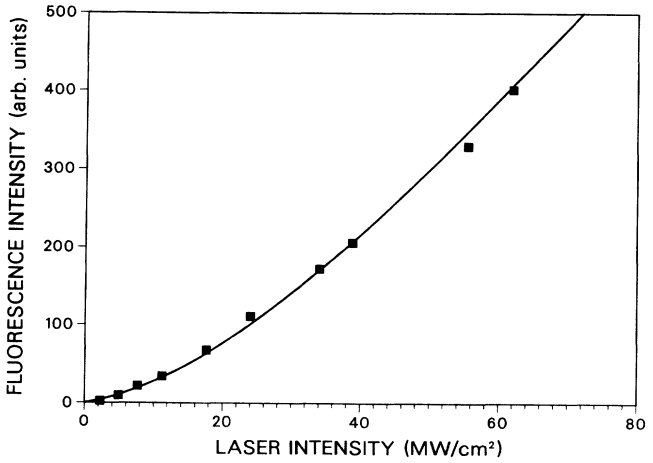

FIG. 4. Excitation-intensity dependence of the fluorescence intensity of emission from the second $J=1$ multiplet in 0.1 at.% Cm^{4+}:CeF_4 at 4 K observed with the dye laser tuned to the 19 949 cm^{-1} component of site A Cm^{4+} (see Fig. 2). The fluorescence intensity data (■) were recorded using a 1-μs wide gate delayed 0.5 μs, with respect to the dye laser pulse. The solid curve is the prediction from a saturation model incorporating one- and two-photon excitation processes.

cm^{-1}, the observed fluorescence intensity is a superposition of emission from one- and two-photon excitation processes. The rapid increase in fluorescence intensity with increasing pumping intensity indicates that the two-photon process is efficient and could dominate the emission at high pump intensity. At high pump intensity, the slope of the curve in Fig. 4 increases but less than expected for one- and two-photon excitation processes, which is indicative of saturation. For sequential absorption of two photons, the excited-state ion densities can be written as[46]

$$n_1 = n_p[1-\exp(-\Delta n_1 \sigma_1 z)] \tag{1a}$$

for first excited state, and

$$n_2 = n_p[1-\exp(-\Delta n_2 \sigma_2 z)] \tag{1b}$$

for second excited state, where $n_p (= L_p \tau / h\nu z)$ is the photon density of the laser field, L_p is the laser intensity, τ is the laser-pulse duration, z is the dimension of the sample, $h\nu$ is the single-photon energy, and σ_1 and σ_2 are the transition cross sections for the first and second steps, respectively. Taking into account saturation for both steps, the ion density differences for the two steps are defined as

$$\Delta n_1 = n_0/(1+L_p/L_{s1}) \tag{2a}$$

and

$$\Delta n_2 = n_1/(1+L_p/L_{s2}) , \tag{2b}$$

where the parameter $L_{s1,2}$ is called the saturation intensity[46] and is a function of the line shape for the corresponding transition. Because of the rapid nonradiative decay of higher-lying states, the ion density in the emitting level is then $n_e = n_1 + n_2$. Using this value for n_e and the assumption that $L_{s1} = L_{s2}$, the observed laser intensity dependence was fit and is shown as a solid curve in Fig. 4. With the stated assumptions, the best-fit values are $L_{s2} = 200$ MW/cm^2 and $\sigma_2 = 8 \times 10^{-18}$ cm^2. The value of σ_1 cannot be determined from the fluorescence intensity data that has arbitrary units.

It is important to note that the one- and two-photon excitation processes can create significant excited-ion densities and substantially deplete the Cm^{4+} ground-state population. High-excited ion densities increase the rate of excited-state processes such as exciton-exciton annihilation, while a reduced ground-state population results in diminished cross relaxation.

IV. SUMMARY OF EXPERIMENTAL RESULTS

Using selective laser excitation, we have measured the fluorescence decays of the metastable $5f$ state ($J = 1$) of Cm^{4+} in CeF_4, using Cm^{4+} concentrations of 0.1 at. % and 5 at. %. The pulsed dye laser beam was partially focused (circa 0.1-mm^2 cross section) on the powder samples and the laser power was varied over the range of 30 to 500 μJ/pulse (i.e., 6–100 MW/cm^2) at the samples. The fluorescence decays were averaged to obtain a signal-to-noise ratio of 100 or more.

We observed efficient excitation-energy transfer among Cm^{4+} ions in the Cm^{4+}:CeF_4 samples even at actinide-ion concentration as low as 0.1 at. %. Nonexponential fluorescence decays of the Cm^{4+} were observed at all laser powers and from 4 to 300 K. Figure 5 shows the observed fluorescence decay of Cm^{4+} ions on sites A and B in the 0.1 at. % sample at 200 K using a laser intensity of circa 60 MW/cm^2. The decay curves were identical for sites A and B at this temperature and had no excitation-intensity dependence. In the 0.1 at. % sample, fluorescence decays were nonexponential at short times and approached a single exponential at long times. Both initial nonexponentialities and long-time single exponential rates of the two ion sites were weakly dependent on temperature. The measured fluorescence-decay time in the long-time region, assumed to be the lifetime of the excited state of isolated Cm^{4+} ions, was identical for sites A and B. In the 5 at. % sample, the fluorescence decay, shown in Fig. 6, was very rapid during the first few μs following excitation and became single exponential at long times. Between the fast initial decay and slow single exponential decay at long time, there was a transition region from 15 to about 50 μs, during which the decay rate decreased by over 2 orders of magnitude. The solid curves in Figs. 5–7 are based on fits to models of cross relaxation, exciton-exciton annihilation, and excitation migration, which are discussed in detail in Secs. V and VI of this paper.

As shown in Figs. 5 and 6, the nonexponential character of the observed fluorescence decays were strongly concentration dependent, as expected when the dominant energy-transfer processes arise from ion-ion interactions. At low temperature, however, the fluorescence decay of Cm^{4+} ions on site A in the 0.1 at. % sample became dependent on excitation intensity and frequency. At 4 K and low excitation intensity (10 MW/cm^2), the site A Cm^{4+} decay was the same as that of site B Cm^{4+}. However, at higher excitation intensity and, therefore,

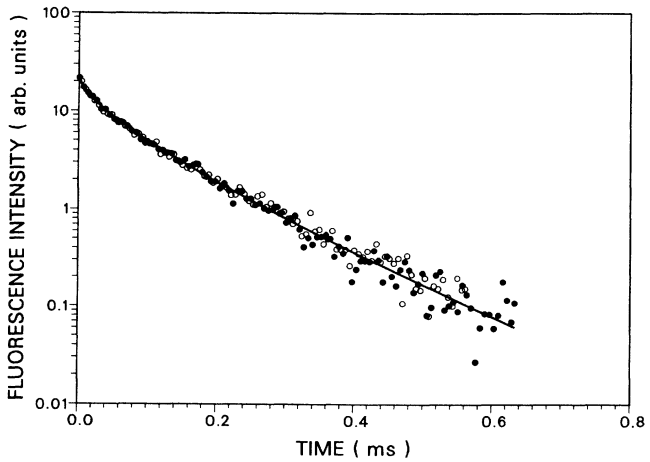

FIG. 5. Time-resolved and site-resolved fluorescence decay of the emitting $J = 1$ multiplet in 0.1 at. % Cm^{4+}:CeF_4 at 200 K observed while monitoring emission to the lower-lying $J = 1$ multiplet. The observed decay data (every tenth data point plotted) are for site A Cm^{4+} (●) and site B Cm^{4+} (○). The solid lines correspond to a cross-relaxation energy-transfer model described in the text.

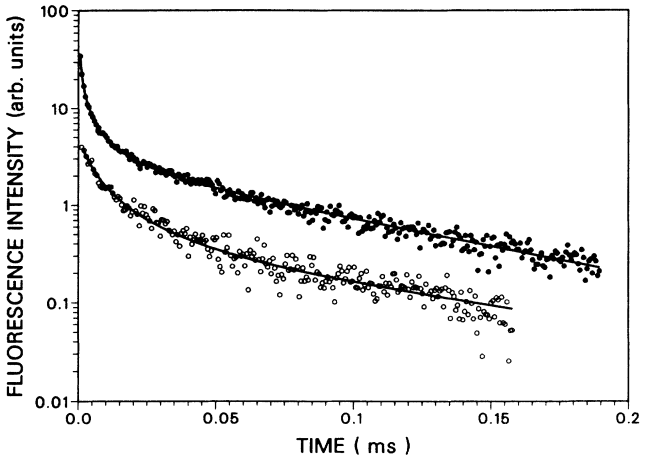

FIG. 6. Excitation-frequency dependence of the fluorescence decay of the emitting multiplet in 5 at. % Cm^{4+}:CeF_4 at 4 K when exciting the third absorption feature (4 cm^{-1} wide) in the emitting multiplet. The data were recorded with the dye laser tuned to line center (●) and tuned to 2 cm^{-1} below line center (○). The excitation intensity was approximately 40 MW/cm^2 in both cases and the solid lines are fits to a dynamics model incorporating exciton-exciton annihilation and energy transfer to traps.

higher-excited ion densities, the site A Cm^{4+} initial nonexponential decay became slower, while the overall decay became faster (see Fig. 7). In contrast, the decay of site B Cm^{4+} exhibited no observable excitation-intensity dependence at 4 K.

The excited-ion density dependence of the fluorescence decay of site A Cm^{4+} at 4 K was studied in an alternative way. Using an 0.03-cm^{-1} line width dye laser and constant laser intensity, we measured Cm^{4+} fluorescence decay as a function of excitation wavelength, while step scanning across the inhomogeneously broadened Cm^{4+} absorption lines. The nonexponential fluorescence decay at short time was slower when the dye laser was tuned to the center of an absorption line, but became faster when the laser was tuned to either the higher or lower frequency side of the line. Variation of excitation frequency across the absorption line (or from a weak to a strong line) produces changes in excited-state density similar to those obtained by varying laser intensity at fixed excitation frequency. At constant laser intensity, the excited-ion density produced depends on the absorption coefficient. Consequently, at the center of the absorption line, more ions are excited than in the two wings of the line.

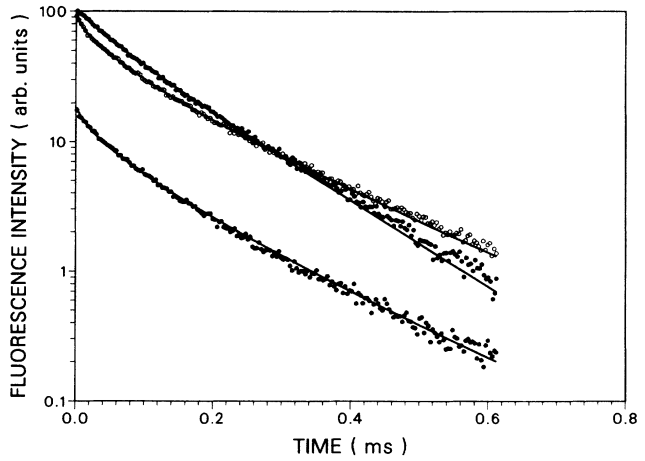

FIG. 7. Excitation-intensity dependence of the site-resolved fluorescence decay of the emitting multiplet in 0.1 at. % Cm^{4+}:CeF_4 at 4 K. Data for site A Cm^{4+} (●) were recorded at 10 MW/cm^2 (lower curve) and 60 MW/cm^2 (upper curve) while pumping the strongest sharp line component of the emitting multiplet of site A Cm^{4+} [see Fig. 2(a)]. Data for site B Cm^{4+} (○) were recoreded at 60 MW/cm^2 while pumping the strongest sharp line component of the emitting multiplet of site B Cm^{4+} [see Fig. 2(b)]. The solid lines through the decay data show the fit to Eq. (6).

For both sites in the 5 at. % sample, a larger excitation density dependence was observed in comparison with that found in the 0.1 at. % sample. The initial decay rate became faster at high-excitation density (i.e., with increasing laser power or tuning the laser frequency across a Cm^{4+} absorption line). Figure 6 shows the excitation density dependence of the fluorescence decay in the 5 at. % sample as the laser frequency was tuned across the absorption line. These observations are analyzed in Sec. VI. Direct transfer to Cm^{4+} traps was observed in the 5 at. % sample by recording emission spectra as a function of delay time with respect to excitation (see Fig. 9).

Cooperative luminescence due to strongly coupled ion pairs was not observed in the Cm^{4+}:CeF_4 samples studied and cooperative pair absorption features like those reported in Pr^{3+}:LaF_3 (Refs. 14 and 47) were absent even in 5 at. % Cm^{4+}:CeF_4. Thus, cooperative pair absorption and emission were not considered in the determination of the energy-transfer mechanisms underlying the observed intensity- and frequency-dependent nonexponential decays.

V. FLUORESCENCE DYNAMICS

A variety of energy-transfer mechanisms were considered in an effort to understand all the features of the observed nonexponential fluorescence decays. As discussed in detail later, cross relaxation, exciton-exciton annihilation, photon-induced site distortion, and transfer to traps all play a role in the observed fluorescence dynamics of the metastable emitting state of Cm^{4+} in CeF_4.

Concerning the physical interactions that influence the dynamics of the excited states of the optical ions doped into solids, ion concentration is often of primary importance. In a very dilute compound, the interaction between dopant ions is negligible. The excited-state dynamics of such a system are dominated by spontaneous emission of photons or nonradiative decay processes induced by interaction with host ions via electron-phonon interaction or fluctuating nuclear moments. As the dopant concentration is increased, for example between 0.1 and 1 at. % for rare-earth compounds,[13,48] coupling between dopant ions can become significant. For such dilute systems, the electromagnetic interaction must be long range since the average ion separation is still large. At higher

concentration, short-range ion-ion interaction becomes increasingly significant.

In the 0.1 at. % Cm^{4+} sample, the average ion separation is about 10 lattice sites (~4.3 nm),[38] which results in largely isolated Cm^{4+} ions except for long-range interactions such as dipole-dipole coupling. In the analysis of fluorescence decay in the 0.1 at. % sample, therefore, only long-range multipole couplings need be considered. However, since the actinide $5f$ electronic states are intermediately extended,[5,8] the effect of the wave-function overlap (i.e., exchange interaction) between neighboring Cm^{4+} ions on the dynamics of the excited $5f$ states in the 5 at. % sample may not be negligible.

If excitation transfer from ion n to ion n' is irreversible, which is expected for cross relaxation and trapping, the dynamics of the excited state via energy transfer has an exact solution[14,49] that results in the fluorescence intensity, $L(t)$, following pulsed excitation, having the form

$$L(t) \propto \exp(-k_0 t)\langle \exp(-\Sigma W_{nn'} t)\rangle_c \ , \tag{3}$$

where t is the time after excitation, k_0 is the reciprocal lifetime of the excited state (assumed to be identical for all ions), $\langle \cdots \rangle_c$ denotes an ensemble average over the crystal lattice of the sample, the summation is over $n' \neq n$, and $W_{nn'}$ is the energy-transfer rate from ion n to ion n'. The value of $W_{nn'}$, based on Forster-Dexter theory,[15,49] for two ions, n and n', separated by a distance $R_{nn'}$, is

$$W_{nn'} = \alpha / R_{nn'}^{s} \ , \tag{4}$$

where the parameter α contains the matraisx elements of the interaction between ions n and n' and s is 6, 8, or 10 for electric dipole-dipole, dipole-quadrupole, or quadrupole-quadrupole interaction, respectively. These matrix elements depend on the transition probabilities as well as the energy mismatches of the energy levels involved.

A. Resonant cross relaxation

If ion-phonon coupling is not involved, the Forster-Dexter theory is directly applicable to actinide ions. In the multipole-multipole description of donor-acceptor energy transfer given in Eq. (4), the matrix elements can be written as products of multipole moments, M_n, of the donor n, and $M_{n'}$, of the acceptor n', between the ground state and excited states[15,49]

$$\alpha \propto |\langle n|M_n|n^*\rangle|^2 |\langle n'^*|M_{n'}|n'\rangle|^2 \ , \tag{5}$$

where the asterisk denotes an excited state. In the case of dipole-dipole coupling, the cross-relaxation rate is thus proportional to the products of optical transition probabilities of donor and acceptor between the involved energy levels. Therefore, the value of the matrix element for cross relaxation can be derived from the observed optical spectra.

The observed emission spectra of the dilute Cm^{4+} samples and the absorption spectra of a concentrated sample[50] indicate that the resonance transition between the metastable emitting state ($J=1$) and the ground state ($J=0$) is at least 3 orders of magnitude weaker than most other observed transitions between the emitting level and lower-energy states or transitions seen in absorption between the ground state and the same low-lying excited states. This provides evidence that the resonance transition, ground state to emitting level, is highly forbidden as an electric dipole transition. The probability of donor-donor resonant energy transfer via electric dipole-dipole interaction is, therefore, small. On the other hand, cross relaxation may be very efficient because of the much higher transition probabilities involved and the availability of resonant and near-resonant cross-relaxation channels. The observed optical line widths for the 0.1 at. % sample at 4 K are 3 to 5 cm^{-1} for the purely electronic transitions between the ground state and components of the emitting $J=1$ multiplet and for emission lines from the emitting level to the components of the low-lying $J=3$ and $J=4$ multiplets, which could be the intermediate states for the resonant cross relaxation. When Cm^{4+} on either site A or site B is excited, there are more than six channels providing cross relaxation with energy mismatches from 0 to 20 cm^{-1} for a pair of Cm^{4+} ions, one initially in the emitting level and the other in its ground state, if the final states of these ions are within the $J=3$ and $J=4$ multiplets. Figure 8 shows the energy levels involved in the most probable cross relaxation paths after a Cm^{4+} on site A is excited. Additional combinations of energy levels involving vibronic components of the $J=0,5,6$ states lying below the emitting level and the electronic levels of the first $J=1,2$ multiplets can also be involved in cross relaxation. As described in detail in Sec. V B, the large number of cross-relaxation pathways with small energy mismatches accounts for the observed, weakly temperature-dependent, nonexponential, fluores-

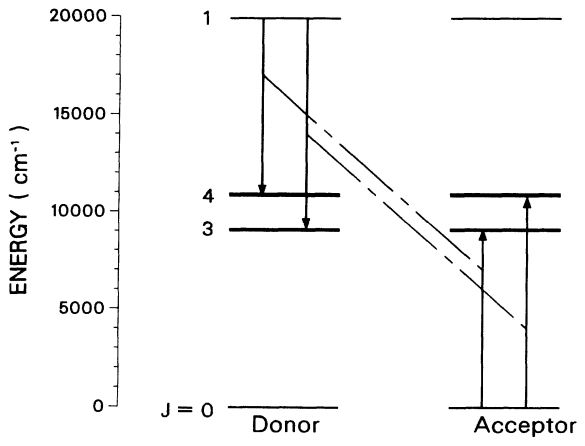

FIG. 8. Resonant electronic cross relaxation via $5f$ states depicted using a partial energy-level diagram for Cm^{4+}:CeF_4. The donor Cm^{4+} ion is initially in the emitting $J=1$ level and the acceptor Cm^{4+} ion is initially in its $J=0$ ground state. As time evolves, cross relaxation occurs, while total electronic-excitation energy is conserved. Two such processes are shown, one in which the donor ion is lowered to its $J=4$ state, while the acceptor ion is raised to its $J=3$ state, and the other in which a $J=3$ state donor and a $J=4$ state acceptor are created.

cence decays observed at low excitation intensity in the 0.1 at. % Cm^{4+} sample.

B. Application to 0.1 at. % Cm^{4+}:CeF_4

In a dilute sample, where there is a broad range of interion distances, the cross-relaxation rate depends on the particular site occupied by the excited ion. If one considers the distance dependence of cross relaxation given in Eqs. 3 and 4, it is evident that energy transfer involving another Cm^{4+} ion is probable only if the acceptor ion lies with a certain spherical volume centered on the donor. This spherical volume is often termed the sphere of influence. Otherwise, an excited Cm^{4+} will lose energy by spontaneous emission of a photon. After an excitation laser pulse, excited Cm^{4+} ions relax either nonradiatively via cross relaxation or radiatively by photon emission. Eventually, most of the remaining excited ions in the emitting state are in isolated sites, at which point in time the fluorescence decay becomes exponential.

In Cm^{4+} cross relaxation, intrinsic Cm^{4+} ions act as both donors and acceptors in the energy-transfer process. Moreover, resonant donor-donor transfer is negligible in this system. Therefore, the dynamics of excited state Cm^{4+} can be described by the irreversible transfer model as discussed before and Eq. (3) can be used directly in fitting the observed fluorescence decays. For a dilute system with constant acceptor density, an integration based on the continuous medium approximation, instead of a crystallographic average, is appropriate and the fluorescence intensity can be written as[14,15,49]

$$L(t)=L(0)\exp(-k_0 t-k_1 t^{3/s}) , \tag{6}$$

where s denotes 6 for dipole-dipole interaction and k_1 is the integrated rate of energy transfer from donor to acceptor. Using Eq. (4), one can derive the following expression for k_1, the energy-transfer rate[14,15,49]

$$k_1=(4\pi/3)R_0^3 n_a W_0^{3/s}\Gamma(1-3/s) , \tag{7}$$

where R_0 is the nearest-neighbor separation, n_a is the acceptor ion density (i.e., ground-state Cm^{4+} ion density), W_0 is the cross-relaxation rate for nearest-neighbors, and s denotes 6 for dipole-dipole coupling.

The observed fluorescence decays of 0.1 at. % Cm^{4+}:CeF_4 are well fit by Eq. (6) with s denoting 6 at all temperatures and excitation densities except for site A at low temperature and high excited ion densities. The solid curve in Fig. 6 is the result of carrying out a nonlinear least-squares fit of Eq. (6) to the observed decay. The fit values for Cm^{4+} on sites A and B at 200 K are $k_0=5.5\times10^3$ s^{-1} and $k_1=1.1\times10^2$ $s^{-1/2}$. Assuming a nearest-neighbor distance of 0.43 nm, the resulting cross-relaxation rate for nearest neighbor Cm^{4+}, W_0, is 2.2×10^8 s^{-1}. For 0.1 at. % Cm^{4+} at 4 K, the fit values of k_0 and k_1 are 3.8×10^3 s^{-1} and 8×10^1 $s^{-1/2}$, respectively, and $W_0=1.2\times10^8$ s^{-1}. The data for site A Cm^{4+}, as shown by the lower curve in Fig. 7, were obtained using a laser intensity of 10 MW/cm^2 and excitation of the highest energy, purely electronic, component of the emitting multiplet.

It is interesting to compare our results for the resonant cross relaxation of Cm^{4+} to reported rates of +3 lanthanide-ion resonant cross relaxation and related phonon-assisted processes. In a recent study of 1 at. % Tb^{3+}:YAG by Bodenschatz *et al.*,[15] a dipole-quadrupole interaction was used to fit the resonant electronic cross relaxation at low temperatures. At $R_0=0.6$ nm, the fit value for W_0 at 1.6 K was 1.18×10^5 s^{-1}. If we use $R_0=0.6$ nm and calculate W_0 for 0.1 at. % Cm^{4+}:CeF_4, the resulting value of W_0 for Cm^{4+} is over 10^2 larger than that for Tb^{3+} in YAG.

Hegarty and co-workers[14] studied 20 at. % Pr^{3+}:LaF_3 and reported a nearest-neighbor cross-relaxation rate of 8.9×10^4 s^{-1} at 2 K rising to 6×10^{10} s^{-1} at higher temperature. These rates apply for an energy mismatch of 190 cm^{-1} and nearest-neighbor distance of 0.4138 nm. If their cross-relaxation rate at 2 K is due solely to electronic interaction, then it is 10^3 smaller than the cross-relaxation rate we have observed for Cm^{4+}:CeF_4.

As the laser intensity is increased to 60 MW/cm^2 for the same excitation transition of site A Cm^{4+}, the initial nonexponential decay, shown as the upper curve for site A in Fig. 7, became slower, while the overall decay became faster. The fit value of k_1 dropped to 3.8×10^1 $s^{-1/2}$, while k_0 increased to 6.8×10^3 s^{-1}. At very high laser intensity, Eq. (6) fails to fit the observed fluorescence-decay data for site A Cm^{4+}. The cross-relaxation model predicts a faster initial decay and a slower exponential at long times than is actually observed at higher laser intensity. In addition, this model did not provide a good fit to the fluorescence-decay data from the 5 at. % sample, making it evident that additional mechanisms need to be taken into account in these cases.

C. Excitation density dependence

To interpret the excitation-density dependent decay of site A Cm^{4+} in the 0.1 at. % sample, processes which depend on excited-ion density must be considered. In Fig. 7, two decay curves of site A Cm^{4+} are plotted on the same scale. The data were recorded under the same experimental conditions except for excitation intensity. It has been noted that as the excited ion population increases, the probability of cross relaxation is reduced due to the correspondingly diminished ground-state population. One might expect, therefore, that the fluorescence decay observed using higher excitation intensity would have a slower initial decay rate. Over the range of laser intensities used, site B Cm^{4+}, however, does not exhibit the same reduction in initial fluorescence-decay rate with increasing excitation intensity. We do not know the absolute absorption cross sections for site A and site B Cm^{4+}, so this observation may arise, at least in part, from a smaller absorption cross section, and consequently reduced ground-state depletion, for site B Cm^{4+}. An additional factor, laser-induced site distortion, should also be considered in this regard.

D. Effect of laser-induced site distortion

As briefly discussed in Sec. III D, only site *A* Cm^{4+} undergoes photon-induced site distortion. We note as well that excitation intensity dependent fluorescence decays were only observed for site *A* Cm^{4+}. This is unlikely to be coincidental. Photon-induced site distortion reduces the density of acceptors for resonant cross relaxation because the site distortion alters the energy-level structure of Cm^{4+} ions on distorted sites. In general, this will increase energy mismatch and reduce the observed cross relaxation rate at low temperature. Experimentally, a 10% reduction in the fluorescence intensity of site *A* Cm^{4+} has been observed due to the accumulation of Cm^{4+} on distorted sites that are thermally stable below 70 K. Typically, the distorted sites were created using an excitation intensity of 60 MW/cm^2 at a 10 Hz laser-pulse rate for 2 min total irradiation time with the dye laser tuned to the highest-energy purely electronic component of the emitting multiplet. Based on modeling of the observed decays using Eq. (6), a 10% reduction in the site *A* Cm^{4+} acceptor population does not fully account for the observed reduction in the site *A* Cm^{4+} fluorescence-decay rate with increasing laser intensity. However, use of Eq. (6) presupposes constant acceptor concentration (i.e., constant ground-state density) during the decay and the data shown in Fig. 4 indicate significant saturation at high-excitation intensity, providing evidence of significant ground-state depletion of site *A* Cm^{4+}.

Modeling of the observed data in terms of cross relaxation requires accounting for the combined effect of reduced site *A* Cm^{4+} density due to formation of distorted sites and depletion of ground state density due to saturation of the absorbing transition. This is a formidable task since the simplifying assumptions used to obtain Eq. (6) from Eq. (3) are not valid when the acceptor concentration varies during the decay. Furthermore, the most probable site for distortion to occur is in an area of large local crystal strain due to high local Cm^{4+} density. On the other hand, because of reduced ion-ion distances, excited Cm^{4+} in such an area, prior to site distortion, would be undergoing cross relaxation at a higher than average rate. If site distortion occurs predominantly in areas of high local Cm^{4+} density and Cm^{4+} ions on distorted sites do not participate in site *A* Cm^{4+} cross relaxation, then site distortion will have a larger than otherwise expected effect due to loss of those site *A* Cm^{4+} ions most likely to undergo cross relaxation.

As noted before, permanent site distortion alone cannot interpret the observed slow cross relaxation rate at high-excitation density. If the reduction in cross relaxation is only due to the permanent site distortion, then the fluorescence decay rate of site *A* Cm^{4+} should be reduced when using low-excitation intensity after the creation of distorted sites using high-intensity excitation. In contrast, after the high-intensity excitation of site *A* Cm^{4+}, fluorescence decays measured at low-excitation intensity still had a faster cross relaxation rate in comparison with the previously recorded high-excitation intensity decay curves. It is likely, therefore, that the combination of several factors contributes to site *A* Cm^{4+} exhibiting a reduced initial decay with increasing excitation intensity. These are (1) a reduction in the ground-state site *A* Cm^{4+} density due to the creation of the distorted site Cm^{4+}, (2) a reduction in the ground state Cm^{4+} due to optical saturation of the absorbing transition, and (3) a site-dependent absorption cross section for the pumped transition.

VI. ENERGY TRANSFER MECHANISMS IN 5 at. % Cm^{4+}:CeF_4

Nonradiative energy-transfer rates increased with Cm^{4+} ion concentration as evidenced by the substantially higher fluorescence quenching found in the 5 at. % Cm^{4+} sample. In the 0.1 at. % sample, as discussed in Sec. V, cross relaxation dominates nonradiative energy transfer and leads to nonexponential fluorescence decays. The rate of cross relaxation given in Eq. (7), derived based on the absence of donor-donor transfer, has a linear dependence on the ion concentration. For this reason, cross relaxation should be more rapid in the 5 at. % sample. However, the observed fluorescence decays in the 5 at. % sample could not be fit by the cross-relaxation model alone. As indicated in Sec. V, the nonexponentiality induced by cross relaxation is an ensemble effect of nonequivalent interactions for individual ioins in a dilute system. As ion concentration increases this nonequivalence is removed, particularly for long-range ion-ion interactions. As a result, the fluorescence decay becomes faster and the overall decay curve tends toward a single exponential. In a stoichiometric compound, the fluorescence decay can become completely single exponential because every ion has an identical environment.

As shown in Fig. 6, the fluorescence decay of 5 at. % Cm^{4+} in CeF_4 can be divided into three time regions. During the first 15 μS, the decay is very rapid. From 15 μs to about 50 μs is a transition region in which the decay rate slows down by more than 2 orders of magnitudes. In the longest time region, the decay became a single exponential whose rate is about the same as that observed in the long-time fluorescence-decay region of the 0.1 at. % sample. This decay pattern is similar to that reported for Nd^{3+}:LaF_3 by Voron'ko *et al.*,[16] who concluded that both resonant donor-donor transfer and donor-acceptor cross relaxation contributed to the observed decay. It is unlikely that donor-donor transfer is important in the fluorescence dynamics of the 5 at. % Cm^{4+} sample because of the very weak temperature dependence of the observed decays. In addition, optical saturation in our system is different because the Cm^{4+} transition between the ground state and the fluorescent state is very weak (although saturation is not important if donor-donor energy transfer is dominated by quadrupole or exchange interactions). Furthermore, the observed transfer of excitation to trap site Cm^{4+} (see Fig. 9) provides evidence of a nonradiative decay pathway not observed by Voron'ko and co-workers.[16] Finally, the large transition probabilities from the fluorescent level to high-energy states from 30 000 to 40 000 cm^{-1}, evidenced by efficient two-photon excitation, forces consideration of up conversion, which is a special cross relaxation process with two coupled ions each initially in an excited state.

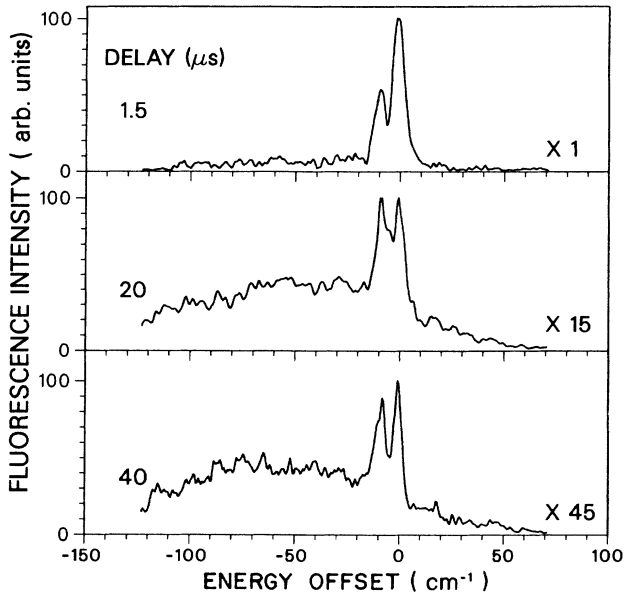

FIG. 9. Excitation migration to trap site Cm^{4+} in 5 at. % Cm^{4+}:CeF_4 at 4 K. The dye laser was tuned to 19 920 cm^{-1}, the center of a zero phonon line of the emitting $J=1$ multiplet of site B Cm^{4+}, and a boxcar integrator with a variable gate delay was used. Zero-energy offset corresponds to the 16 584 cm^{-1}, the center of a site B Cm^{4+} zero-phonon emission transition to the lowest-energy component of the lower-lying $J=1$ state. The broad band, which grows in with increasing delay time, is attributed to emission from trap site Cm^{4+} and the shift of its peak intensity provides evidence of energy migration from higher to lower energy traps.

A. Exciton-exciton annihilation

As analyzed earlier, exciton-exciton annihilation may play a significant energy transfer role in the 5 at. % Cm^{4+} sample. Because of a high density of states and the small energy gaps above the initially excited state, the up-converted ions rapidly relax and most of them evidently reoccupy the initially excited state. Using excitation laser energies as high as 26 400 cm^{-1}, no additional emitting level was found above the fluorescent metastable level at 19 910 cm^{-1}, even though there is an energy gap larger than 1000 cm^{-1} between the fluorescent level and the lowest component of the next higher multiplet. When using excitation energy as high as 26 400 cm^{-1}, the observed rise time of fluorescence from the emitting level was 10 ns. This is comparable with the laser-pulse duration. According to a predicated Cm^{4+} energy-level structure,[51] there is no energy gap larger than 1000 cm^{-1} between purely electronic states from 26 000 to 40 000 cm^{-1}. The lack of observable emission from higher-lying states renders direct fluorescence detection of up conversion impractical in this system. It is clear, however, that fast relaxation from higher-lying states occurs and refills the emitting state following exciton-exciton annihilation.

Experimental support for exciton-exciton annihilation is found in the observed excitation density dependence. Excitation density was varied by altering the dye laser power or by tuning the excitation frequency across the transition line. In the two wings of the line or at low laser intensity, the initial fast decay was reduced, which prevented a clear separation of the decay into an initial fast section, a transition region, and a single exponential decay. Figure 6 shows the observed decay curves for excitation in the center and low-energy wing of the absorption line of the Cm^{4+} ion in the 5 at. % sample. The nonexponential decay rate was still high when exciting in the wing of the line in comparison with the decay curves in the 0.1 at. % sample.

Based on the preceeding considerations, we can describe the dynamics of excited state Cm^{4+} in 5 at. % Cm^{4+}:CeF_4 by using a simple rate equation in which all ions are assumed to have the same transition probability:[23,26,27]

$$dn/dt=-k'n-\gamma n^2+(\epsilon/2)\gamma n^2 , \tag{8}$$

where n is the excited ion density, k' is the summation of the reciprocal lifetime, the rate of cross relaxation, and the rate of excitation transfer to traps, γ is the coefficient of exciton-exciton annihilation, and ϵ is the fraction of refilling of the emitting state from higher-lying levels.

B. Excitation migration

An additional excitation transfer mechanism arises because of the existence of minor defect sites and traps, some of which likely result from radiation damage due to alpha decay or fission of ^{248}Cm. Defect sites were barely detectable in the 0.1 at. % sample. The spectral intensities of features attributed to trap sites were more than 3 orders of magnitude weaker than those of the major sites and had separable line structure. In the 5 at. % Cm^{4+} sample, however, energies of traps were continuously distributed on both the low- and high-energy sides of the intrinsic ion sites (see Fig. 9). The peak trap emission intensity was weaker than the intensity of intrinsic ions, but comparing the integrated areas of the emission spectra and assuming equal transition probabilities for trap and major site ions, the total number of traps is comparable with the total numbers of ions on the major sites. In addition, clear evidence of spectral migration from high to low frequencies of the trap emission was observed in the time-resolved emission spectra after an excitation of intrinsic site B Cm^{4+} as shown in Fig. 9.

To describe the dynamics of the trap states, energy transfer from the intrinsic site to the trap sites as well as energy transfer among the trap sites need to be taken into account. The irreversible transfer model, as used for cross relaxation in the 0.1 at. % sample, is appropriate here to describe the energy transfer among the trap sites because of the glasslike site-energy distribution,[12] but the rate equation is not integrable because there is a nonexponential feeding source term. Taking this term into account, the time dependence of the density of excited traps n' whose energy is near the intrinsic line can be written as

$$dn'/dt=-k'_0n'+k'_1(t)n(t)-k'_2(t)n' , \tag{9}$$

where k'_0 is the reciprocal lifetime of trap emission, $k'_1(t)$ is the rate of transfer from excited intrinsic site ions of

density $n(t)$, and $k_2'(t)$ is the rate of transfer to other trap sites. With direct excitation on trap sites, we found that the fast decay region at short times was absent in the fluorescence decays of the trap emission. As a test of the dominance of cross relaxation in the decay of 5 at. % Cm^{4+}, the cross-relaxation model derived in Sec. V was used in combination with trap emission to fit the fluorescence decays in the 5 at. % sample. This approach was unsuccessful because the initial fast decay and transition regions could not be fit simultaneously with any variation of all parameters. Combining all of the facts we have discussed in Sec. VI, we have fit the observed 5 at. % Cm^{4+} decay curves using Eqs. (8) and (9) as described later.

C. Fitting fluorescence decays in 5 at. % Cm^{4+}:CeF_4

Since trap emission covers a range of over 100 cm^{-1} and overlaps intrinsic ion emission, the contribution of the trap emission to the observed fluorescence had to be taken into account when the fluorescence decays were fitted. To do this we simply assume that the observed fluorescence intensity $L(t)$ is the superposition of intrinsic ion emission, $L_n(t)$, and trap ion emission, $L_{n'}(t)$

$$L(t)=L_n(t)+L_{n'}(t) , \tag{10}$$

where the fluorescence intensities $L_n(t)$ and $L_{n'}(t)$ are proportional to the excited ion densities $n(t)$ and $n'(t)$, respectively. To find functional forms for $n(t)$ and $n'(t)$, additional assumptions were necessary. The relaxation of Cm^{4+} ions from energies above the emitting level after up conversion to levels below the emitting level were assumed to be negligible [i.e., $\epsilon=1$ in Eq. (8)] giving

$$n(t)=\frac{2n(0)k'}{[2k'+n(0)\gamma]\exp(k't)-n(0)\gamma} . \tag{11}$$

This is reasonable based on the small energy gaps from state to state from higher energy to the emitting state. From the data in Figs. 6 and 9, one can conclude that most excitation transfer from intrinsic ions to traps occurs in the fast decay region (0–15 μs) and has negligible effect on the observed fluorescence after this time period. Therefore the second term in Eq. (9) could be approximated by a constant so that $n'(t)$ has the same form as Eq. (6):

$$n'(t)=n'(0)\exp(-k_0't-k_2't^{1/2}) , \tag{12}$$

where k_2' is the excitation-migration rate. Furthermore, we define the initial trap density, $n'(0)$, as $n'(0)=xn(0)$, where $n(0)$ is the initial intrinsic ion excited-state density and x is a dimensionless parameter to be fit by nonlinear least-squares adjustment.

Using Eqs. (11) and (12) and fitting the fluorescence-decay data for various excitation densities as the laser was tuned across the line center of the 5 at. % sample at 4 K (see Fig. 6), we obtained $x=0.02$ at the center of the absorption and 0.1 in the wings at 2 cm^{-1} from line center. The fit value of k', 5×10^4 s^{-1}, is more than 1 order of magnitude larger than k_0, the reciprocal lifetime of the isolated Cm^{4+}, which is attributed to trapping and cross-relaxation processes. The value of the exciton-exciton annihilation coefficient γ as fit, was 1×10^{-14} cm^3s^{-1} with a factor of 5 uncertainty due to the uncertainty in $n(0)$ that was fixed as 4×10^{18} cm^{-3} for excitation at line center. The fit value of the k_0' was 9.1×10^3 s^{-1} and the fit value k_2', the trap transfer rate, was 3×10^2 $s^{-1/2}$. As expected, the values of parameters k_0' and k_2' primarily influenced the fit in the long-time region of the decay curves.

The fit value of the exciton-exciton annihilation coefficient for the 5 at. % sample is about 1.5 orders of magnitude smaller than that reported 5×10^{-13} cm^3s^{-1} for MnF_2 (Ref. 24) and is about 1 order of magnitude larger than that reported for the stoichiometric lanthanide compounds $TbPO_4$ (Ref. 26) and TbF_3 (Ref. 27). Note that the annihilation coefficient is proportional to the donor density.[9] Thus the expected annihilation coefficient for a concentrated actinide Cm^{4+} compound is more than 2 orders of magnitude larger than that for the lanthanide compounds, and close to the reported value for the transition metal compound.

Within the framework of a random-walk model for diffusion-limited transport of excited states,[52] the annihilation coefficient γ is expressed as $\gamma=8\pi D\langle R\rangle$, where $\langle R\rangle$ is the average interaction radius. Setting $\langle R\rangle$ equal to the mean separation between Cm^{4+} ions in the 5 at. % sample ($\sim$1.2 nm) and using the measured value of γ, the calculated maximum excited-state diffusion coefficient is $D=3\times10^{-9}$ cm^2s^{-1}. On the other hand, the excited-state diffusion coefficient can be estimated from k', the rate of trapping and cross relaxation of the $J=1$ excited state. Following Van der Ziel *et al.*,[53] we estimate the diffusion coefficient from k' and find $D=1\times10^{-9}$ cm^2s^{-1}. These two values for the excited-state diffusion coefficient are identical, taking into account the large uncertainty in γ. Thus, as expected for this disordered system, the dynamics of the excited states are consistently described by the incoherent diffusion-limited energy-transfer model.

VII. CONCLUSIONS

In summary, we have observed complicated excited-state dynamics in studies of the tetravalent actinide ion Cm^{4+} in CeF_4. Nonexponential fluorescence decays, which depend on actinide-ion concentration, excitation intensity, excitation frequency, and photoinduced site distortion, have been analyzed based on the mechanisms of cross relaxation, up conversion, and excitation migration.

Our results indicate that the energy-transfer rates for $5f$ states of Cm^{4+} via cross relaxation and up-conversion processes are 2 orders of magnitude higher than those of lanthanide-activated materials at equal ion density. The larger energy-transfer rates shown by Cm^{4+} are attributed to the extended character of $5f$ electron orbitals, which results in strong ion-lattice coupling as well as increased ion-ion interaction. The dense energy-level structure of Cm^{4+} influences the observed energy-transfer processes. These energy-transfer processes, together with the transfer of energy to the trap sites, significantly quench fluorescence in the 5 at. % Cm^{4+} in the CeF_4 sample. The unusual energy-level structure of Cm^{4+} also enables two-photon excitation leading to population of

the fluorescent state and thereby impacts the observed energy-transfer processes.

ACKNOWLEDGMENTS

We thank C. W. Williams for preparing and characterizing the samples, W. T. Carnall for helpful discussions concerning +4 actinide-ion energy-level structure, and the transplutonium elements production facilities at Oak Ridge National Laboratory for supplying the ^{248}Cm used in this work. This work was performed under the auspices of the Office of Basic Energy Sciences, Division of Chemical Sciences, U.S. Department of Energy, under Contract No. W-31-109-ENG-38.

[1]For recent reviews of lanthanide-ion spectroscopy and energy transfer see *Spectroscopy of Crystals Containing Rare-Earth Ions,* edited by A. A. Kaplyanskii and R. M. Macfarland (North-Holland, Amsterdam, 1987).

[2]For reviews of energy transfer and spectroscopy see *Laser Spectroscopy of Solids,* Vol. 49 of *Topics in Applied Physics,* edited by W. M. Yen and P. M. Selzer (Springer-Verlag, Berlin, 1986).

[3]J. C. Wright, *Radiationless Processes in Molecules and Condensed Phases,* Vol. 15 of *Topics in Applied Physics,* edited by F. K. Fong (Springer-Verlag, Berlin, 1976), Chap. 4.

[4]S. Hufner, *Optical Spectra of Transparent Rare Earth Compounds* (Academic, New York, 1978).

[5]W. T. Carnall and H. M. Crosswhite, Argonne National Laboratory Report No. ANL-84-90, 1985 (unpublished).

[6]M. J. Weber, in *Lanthanide and Actinide Chemistry and Spectroscopy,* Volume 131 of the ACS Symposium Series, edited by N. M. Edelstein (American Chemical Society, Washington, D.C., 1980), pp. 275–311.

[7]J. P. Hessler and W. T. Carnall, in *Lanthanide and Actinide Chemistry and Spectroscopy,* Volume 131 of the ACS Symposium Series, edited by N. M. Edelstein (American Chemical Society, Washington, D.C., 1980), pp. 349–368.

[8]J. C. Krupa, Inorg. Chim. Acta **139**, 223 (1987).

[9]D. L. Huber, in *Laser Spectroscopy of Solids,* Ref. 2, pp. 81–111.

[10]W. M. Yen and P. M. Selzer, in *Laser Spectroscopy of Solids,* Ref. 2, pp. 141–188.

[11]W. M. Yen, in *Spectroscopy of Crystals Containing Rare-Earth Ions,* edited by A. A. Kaplyanskii and R. M. Macfarlane (North-Holland, Amsterdam, 1987), pp. 185–249.

[12]T. T. Basiev, V. A. Malyshev and A. K. Przhevuskii, in *Spectroscopy of Crystals Containing Rare-Earth Ions,* Ref. 1, pp. 275–341.

[13]R. L. Cone and R. S. Meltzer, in *Spectroscopy of Crystals Containing Rare-Earth Ions,* edited by A. A. Kaplyanski and R. M. Macfarland (North-Holland, Amsterdam, 1987), pp. 481–556.

[14]J. Hegarty, D. L. Huber, and W. M. Yen, Phys. Rev. B **25**, 5638 (1982); **23**, 6271 (1981).

[15]N. Bodenschatz, R. Wannemacher, and J. Heber, J. Lumin. (to be published).

[16]Yu. K. Voron'ko, T. G. Mamedov, V. V. Osiko, A. M. Prokhorov, V. P. Sakun, and I. A. Shcherbakov, Zh. Eksp. Teor. Fiz. **71**, 478 (1976) [Sov. Phys.—JETP **44**, 251 (1976)].

[17]D. Fay, G. Huber, and W. Lenth, Opt. Commun. **28**, 117 (1979).

[18]M. Inokuti and F. Hirayama, J. Chem. Phys. **43**, 1978 (1965).

[19]R. G. Kepler, J. C. Caris, P. Avakian, and E. Abramson, Phys. Rev. Lett. **10**, 400 (1963).

[20]V. Ern, H. Bouchriha, M. Bisceglia, S. Arnold, and M. Schott, Phys. Rev. B **8**, 6038 (1973).

[21]A. Bergman, M. Levine, and J. Jortner, Phys. Rev. Lett. **15**, 593 (1967).

[22]T. Kobayashi and S. Nagakura, Mol. Phys. **24**, 695 (1972).

[23]B. A. Wilson, J. Hegarty, and W. M. Yen, Phys. Rev. Lett. **41**, 268 (1978).

[24]E. Strauss, W. J. Maniscalco, W. M. Yen, U. C. Kellner, and V. Gerhardt, Phys. Rev. Lett. **44**, 824 (1980).

[25]W. D. Partlow, Phys. Rev. Lett. **21**, 90 (1968).

[26]P. C. Diggle, K. A. Gehring, and R. M. Macfarlane, Solid State Commun. **18**, 391 (1976).

[27]M. F. Joubert, B. Jacquier, and R. Moncorge, Phys. Rev. B **28**, 3725 (1983).

[28]V. V. Ovsyankin and P. P. Feofilov, Pis'ma Zh. Eksp. Teor. Fiz. **3**, 494 (1966) [JETP Lett. **3**, 322 (1966)].

[29]D. J. Zalucha, J. C. Wright, and F. K. Fong, J. Chem. Phys. **59**, 997 (1973).

[30]D. J. Zalucha, J. A. Sell, and F. K. Fong, J. Chem. Phys. **60**, 1660 (1973).

[31]R. A. Hewes and J. F. Sarver, Phys. Rev. **182**, 427 (1969).

[32]J. P. Hessler, R. Brundage, J. Hegarty, and W. M. Yen, Opt. Lett. **5**, 348 (1980).

[33]A. Milicic, P. Delamoye, and J. C. Krupa, J. Lumin. (to be published).

[34]G. K. Liu and J. V. Beitz, J. Lumin. (to be published).

[35]R. A. Gottscho, Rev. Sci. Instrum. **56**, 529 (1985).

[36]B. A. Palmer, R. A. Keller, and R. Engleman, Jr., Los Alamos National Laboratory Report No. LA-8251-MS, 1980 (unpublished).

[37]L. Stein, E. Rudzitis, and J. L. Settle, Argonne National Laboratory Report No. ANL-6364, 1961 (unpublished).

[38]A. C. Larson, R. B. Roof, Jr., and D. T. Cromer, Acta Crystallogr. **17**, 555 (1964).

[39]D. D. Ensor, J. R. Peterson, R. G. Haire, and J. P. Young, J. Inorg. Chem. **43**, 1001 (1981).

[40]G. K. Liu and J. V. Beitz (unpublished).

[41]H. A. Jahn and E. Teller, Proc. R. Soc. London, Ser. A **161**, 220 (1937).

[42]R. Englman, *The Jahn-Teller Effect in Molecules and Crystals* (Wiley, New York, 1972), pp. 124–146.

[43]G. K. Liu, J. V. Beitz, and W. T. Carnall (unpublished).

[44]J. E. Bjorkholm and P. F. Liao, Phys. Rev. Lett. **33**, 128 (1974).

[45]J. Huang, G. K. Liu, and R. L. Cone, Phys. Rev. B **39**, 6348 (1989).

[46]A. Yariv, *Quantum Electronics,* 2nd ed. (Wiley, New York, 1975), pp. 149–175.

[47]R. Buisson and J. C. Vail, J. Phys. Lett. **42**, L115 (1981).

[48]G. K. Liu and R. L. Cone, Phys. Rev. B **41**, 6193 (1990).

[49]D. L. Huber, D. S. Hamilton, and B. Barnett, Phys. Rev. B **16**, 4642 (1977), D. L. Huber, *ibid.* **20**, 2307 (1979).

[50]W. T. Carnall (unpublished).

[51]W. T. Carnall, G. L. Goodman, C. W. Williams, S. Lam, and G. M. Jursich, J. Less-Common Met. **148**, 201 (1988).

[52]J. Jortner, S. A. Rice, J. L. Katz, and S. Choi, J. Chem. Phys. **42**, 309 (1965).

[53]J. P. van der Ziel, L. Kopf, and L. G. Van Uitert, Phys. Rev. B **6**, 615 (1972).